High-throughput identification of genes involved in single and multi-drug resistance in pancreatic cancer with pooled CRISPR screening

Author list:
Ryne C. Ramaker*[1,2]
Andrew A. Hardigan*[1,2]
Emily R. Gordon[2]
Richard M. Myers[2]
Sara J. Cooper[2]

*These authors have contributed equally to this work

Corresponding author: Sara J. Cooper, sjcooper@hudsonalpha.org

Affiliations: [1]University of Alabama-Birmingham, Birmingham, AL 35294. [2]HudsonAlpha Institute for Biotechnology Huntsville, AL 35806

SUMMARY

Chemoresistance is the norm in pancreatic ductal adenocarcinoma (PDAC) leading to an abysmal five-year survival rate of less than 10%. We performed genome-wide CRISPR activation (CRISPRa) and CRISPR knock out (CRISPRko) screens to identify mechanisms of resistance to four cytotoxic chemotherapies (gemcitabine, 5-fluorouracil, irinotecan, and oxaliplatin) used to treat PDAC patients in two PDAC cell lines. Mirroring patient treatment outcomes, we found that multi-drug resistance genes were more likely to be associated with patient survival. We identified activation of *ABCG2,* a well-described efflux pump, as the most consistent resistance gene in four drugs and two cell lines. Small molecule inhibitors of ABCG2 restored sensitivity to chemotherapy. Our screen demonstrated that activation of members of the hemidesmisome complex and transcriptional repressor complexes conferred resistance to multiple drugs. Finally, we describe an approach for applying our results to predict drug sensitivity in PDAC tumors and cell lines based on gene expression.

KEYWORDS:

Genome-wide screen; CRISPR; pancreatic cancer; drug resistance; ABCG2; modeling drug resistance; precision oncology

INTRODUCTION

The era of high-throughput genome sequencing has led to an unprecedented understanding of the genetic and epigenetic alterations underlying the most common cancers (Kandoth et al., 2013; Sanchez-Vega et al., 2018). In several cases this has led to the development of successful targeted therapies. Early examples such as the *BCR-ABL* gene fusion,

which can be targeted with the tyrosine kinase inhibitor imatinib (Goldman and Melo, 2003), and *EGFR* kinase domain mutations, which have been inhibited with gefitinib (Pao et al., 2004), have been followed by a rapidly growing number of promising targeted therapeutics (Bollag et al., 2012; Katzel et al., 2009; Warr and Shore, 2008). Unfortunately, pancreatic ductal adenocarcinoma (PDAC) has remained largely refractory to the improvement seen in several other cancers with five-year survival rates still less than 10% (Siegel et al., 2018). With largely non-specific symptoms and invasive procedures required for diagnosis, only 20% of PDAC patients are eligible for surgical resection, leaving a majority of patients with chemotherapy and radiation as their sole course of treatment (Kamisawa et al., 2016). Even patients eligible for surgical resection tend to have recurrent disease within 2 years that is refractory to adjuvant chemotherapy (Stathis and Moore, 2010). In an effort to improve patient outcomes, multi-drug combinations such as FOLFIRINOX (fluorouracil, folinic acid, irinotecan and oxaliplatin) are increasingly being used despite associated toxicities and modest improvements in outcomes (Conroy et al., 2011).

Large cohort sequencing efforts have established a relatively short list of commonly mutated genes, including *KRAS*, *TP53*, *SMAD4*, and *CDKN2A*, however these have thus far proven to be poor drug targets (Bailey et al., 2016; Raphael et al., 2017; Witkiewicz et al., 2015). Moreover, few genetic perturbations have been reproducibly associated with patient prognosis (Shugang et al., 2016; Witkiewicz et al., 2015). Transcriptomic sequencing has been more successful identifying subtypes of PDACs that may predict prognosis (Bailey et al., 2016; Collisson et al., 2011; Moffitt et al., 2015; Raphael et al., 2017). Of particular interest, is the squamous/quasi-mesenchymal subtype, which consistently exhibits significantly poorer prognosis than other subtypes. Unfortunately, patient subtyping is based on the expression levels

of thousands of genes in primary tumor tissue, making the delineation of individual targets difficult.

Complete resistance to potent multi-drug cocktails is common in PDAC patients (Garrido-Laguna and Hidalgo, 2015). Several extra-cellular mechanisms for drug resistance have been proposed including a highly immunosuppressive micro-environment (Bazhin et al., 2013), extensive desmoplasia (Chu et al., 2007), and hypovascularization (Koong et al., 2000). Tumor heterogeneity is another notable mechanism of resistance (Yachida and Iacobuzio-Donahue, 2009). PDAC tumors often consist of several unique clonal populations each of which may harbor a genetic background capable of conferring drug resistance and have the potential to become the dominant tumor population after drug treatment. However, these clones are almost impossible to detect in an agnostic manner *a priori* without extremely deep levels of sequencing that are cost prohibitive in most settings (Griffith et al., 2015). An alternative approach to this problem is to define the landscape of cellular mechanisms of PDAC drug resistance experimentally, then deeply screen tumors in a targeted manner for the presence of previously identified resistance drivers. Previous insertional mutagenesis- and RNA interference-based screens have successfully identified novel genes whose inactivation leads to gemcitabine sensitivity in PDAC cells (Bhattacharjee et al., 2014; Smith et al., 2014; You et al., 2011). More recently, genome-wide CRISPR-Cas9 screening, which provides complimentary information to previous screening methodologies (Evers et al., 2016; Morgens et al., 2016), for essential genes across *RNF43*-mutant and wild type PDAC cell lines found mutant lines to be specifically dependent upon *FZD5* despite non-aberrant expression of *FZD5* or other FZD receptors (Steinhart et al., 2017). We performed CRISPR-Cas9 knock-out (CRISPRko, Wang et al., 2014) and endogenous activation (CRISPRa, Konermann et al., 2015) screening in two PDAC cell lines

(BxPC3 and Panc-1) to identify genes whose loss or gain of expression were able to modulate sensitivity to four of the most common cytotoxic chemotherapies used in the treatment of PDAC (gemcitabine, oxaliplatin, irinotecan, and 5-fluorouracil). We identified several novel genes and pathways that contribute to drug specific or multi-drug resistance. We validated our top hits in three cell lines using multiple sgRNAs. We determined that many of our hits are likely relevant to PDAC patients as their expression levels are correlated with overall survival. Finally, we used our screen results to develop a simple algorithm for predicting drug sensitivity in cell lines and patients.

RESULTS

CRISPR screening reveals drug resistance genes

We performed genome-wide CRISPRko and CRISPRa screening in the Panc-1 and BxPC3 cell lines to identify both drug-specific and multi-drug mechanisms of resistance to four drugs commonly used to treat PDAC (gemcitabine, oxaliplatin, irinotecan, and 5-fluorouracil) (Figure 1A, Figure S1). Drug doses were optimized to inhibit growth to a level of 10-20% of the untreated cells although a broader range of selection strength was observed in some cases (Figure S2). We found the sgRNA $\log_2$ fold changes (treated/untreated) of drug replicates were significantly more correlated than samples treated with different drugs (Figure S3). However, there was a much higher correlation between samples treated with different drugs than expected by chance suggesting mechanisms of resistance were sometimes shared between drugs (Figure S3). The degree of replicate agreement also exhibited a strong inverse correlation with drug selection strength (Rho = -0.55, P=0.026, Figure S4). Clustering replicates by the most variable sgRNAs highlights that the strongest mechanisms of resistance are drug-specific, however the

two nucleoside analogs, 5-fluorouracil and gemcitabine, share a relatively large number of top sgRNAs (Figure 1B, Table S1). For example, over-expression of SLC29A1, a nucleoside transporter that is capable of both influx and efflux, confers significant resistance to gemcitabine and 5-FU, but little resistance to oxaliplatin or irinotecan. Other genes showing similar patterns include FMO5, a flavin-containing monooxygenase involved in metabolism xenobiotics that has been linked to prognosis in colorectal cancer (Zhang et al., 2018); several genes that function in cellular metabolism: SCD5, HYAC1, COQ6; and other genes involved in transport or its regulation, SLC22A9, SLC16A7, CCZ1, TBC1D3I.

Drug-specific mechanisms clustered into pathways, some of which were previously described. For example, *TGFB1*-dependent activation of the SMAD regulatory complex has been associated with oxaliplatin resistance (Mao et al., 2017; Sun et al., 2017) and hedgehog signaling has been linked to irinotecan resistance (Meng et al., 2015; Tripathi et al., 2014). Biosynthesis of heme and several phospholipid molecules were pathways uniquely associated with resistance to our nucleoside analogs. Both of these metabolic pathways have been described as important mechanisms of gemcitabine resistance and likely play a role in oxidative stress response (Miyake et al., 2010; Tadros et al., 2017). Overall, we saw that there was a weak positive correlation between enrichment across our screens and patient survival. We determined that this correlation was driven primarily by associations between survival and enrichment in multi-drug resistance genes. We observed that genes enriched in individual drug screens tended to be depleted for significant associations with PDAC patient survival (Figure S5). Based on this result and the fact that PDAC patients are routinely treated with complex drug cocktails, we focused the remaining analysis on multi-drug resistance mechanisms under the assumption that they may hold greater clinical relevance.

To prioritize resistance genes, we computed the sum of the replicate minimum $\log_2$ fold change of the two most enriched sgRNAs targeting each gene (L2FC sum) in each cell line (Table S2A-B). This approach requires that prioritized genes have a large increase in representation for two independent sgRNAs in each replicate and produces a relatively conservative list of hits. Multi-drug resistance genes were identified by computing the mean L2FC sum across all four drugs in each cell line. This approach was particularly powerful as it leveraged information from 48 experiments (4 drug screens x 3 replicates x 2 cell lines x 2 sgRNAs). We found L2FC sums to be weakly correlated across cell lines (rho=0.014, P=0.034), likely a reflection of strong phenotypic and genetic differences found between our two cell lines (Kim et al., 2014).

ABCG2 over-expression confers drug resistance

A subset of genes possessed high L2FC sums in both cell lines. We performed validation experiments on several genes nominated by our screening data in three cell lines, Panc-1, BxPC-3, and MiaPaca-2. These experiments showed evidence for 8 genes conferring resistance with at least one guide in at least one cell line. Overall, 10% of CRISPRko and 22.7% of CRISPRa screens showed statistically significant validation as measured by increased EC50 (Table S3, Figure S6A). In the CRISPRa system, we observed that guides that resulted in a high degree of over-expression were more likely to significantly affect EC50 (Figure S6B).

The top multi-drug resistance gene identified by our CRISPRa screen and validated using independent guides in multiple cell lines was the ATP-binding cassette (ABC) transporter, *ABCG2* (Figure 2A). This gene has been associated with multi-drug resistance primarily in breast cancer, and to some extent in pancreatic cancer cell lines (Bhagwandin et al., 2016; Mo and Zhang, 2012; Sun et al., 2016). *ABCG2* functions as an efflux pump with broad range substrates

and our screen data supported these observations with CRISPRa-mediated activation of *ABCG2* promoting resistance to all four drugs in our screen (Figure 2B). In our screen, *ABCG2* activation led to particularly strong resistance to oxaliplatin treatment, with a six-fold enrichment observed for the top *ABCG2* sgRNA in treated relative to control cells. This sgRNA was capable of increasing *ABCG2* expression to approximately 25 times the baseline expression level exhibited in control cells expressing a scrambled sgRNA and recapitulated the effect observed in the pooled screen in an individual sgRNA validation experiment using a different two vector CRISPRa system (Figure 2C,D). RNA-sequencing data does not suggest significant off-target effects (Figure S7). Furthermore, treatment with KO143 and sorafenib, two inhibitors of ABCG2, was able to reverse the resistance to irinotecan observed in the context of ABCG2 over-expression (2E, Allen et al., 2002; Wei et al., 2012).

Although *ABCG2* activation proves to be a robust mechanism for multi-drug resistance, its expression level is not strongly correlated with patient survival suggesting it may not be a common mechanism of drug resistance in PDAC patients (Figure S8). Nonetheless, ABCG2 is expressed at levels above background with expression increased in some patients for whom our findings may be relevant.

Novel pathways are associated with multi-drug resistance

Examination of top genes in our CRISPRa and CRISPRko screens revealed enrichment of genes involved in a set of Reactome pathways. Many of these pathways also contain genes whose expression was associated with PDAC patient survival (Figure 3A-B, Table S4). These pathways, which when activated induce drug resistance and when knocked out confer drug sensitivity, represent potentially useful therapeutic targets. One pathway meeting these criteria is the hemidesmosome assembly pathway (Figures 4A, S8). The hemidesmisome is a multi-protein

complex that adheres epithelial cells to the basement membrane (Walko et al., 2015) and has been strongly linked to cell adhesion-mediated drug resistance (CAM-DR, Correia and Bissell, 2012). One of the strongest hits in this pathway, *PLEC*, acts as a linker protein for cytoskeletal scaffolding and has been previously associated with BRCA2 activity in breast cancer (Figure S9, Niwa et al., 2009). Several genes in the hemidesmosome pathway show enrichment in our screen (Figure 3C). Our validation results showed PLEC activation was most associated with oxaliplatin resistance in MiaPaca-2 and BxPC-3 cell lines (Figure 3D). In patients, genes of this pathway were highly expressed in the squamous subtype of PDAC, which was described as conferring a particularly poor prognosis (Figure 3E, Bailey et al., 2016). The mean expression level of genes in this pathway was also significantly greater in treatment naïve tumors from PDAC patients who succumbed to disease within 300 days (bottom quartile) relative to those who survived greater than 900 days (top quartile) in two independent cohorts (Figure 3F, Kirby et al., 2016; Raphael et al., 2017). These data nominate the hemidesmosome as potential driver of poor prognosis of the squamous subtype.

Activation of several genes involved in chromatin remodeling also fostered drug resistance (Figure 3A,B). The role of chromatin remodeling in pancreatic cancer has been heavily investigated as several genes involved in histone methylation (*MLL2* and *MLL3*) and members of the tumor suppressing SWI/SNF complex (*SMARCA1* and *ARID1A*) are recurrently mutated in PDAC tumors (Ryan et al., 2014). Moreover, global changes in repressive histone marks has been associated with metastatic PDAC tumors (McDonald et al., 2017). We found that activation of several genes involved in the repression of chromatin via histone deacetylation resulted multi-drug resistance (Figure S10A). Particularly prominent were members of the Nucleosome Remodeling Deacetylase (NuRD) complex (*MTA2/3*, *CHD3/4*, *HDAC1/2,* and

GATAD2A), members of the Nuclear receptor CoRepressor (NCoR) complex (*NCOR2*, *TBL1XR1*, and *TBL1X*), and the repressive transcription factor *REST* and its interacting partner *RCOR1*, each of which have been demonstrated to regulate gene expression programs important for chemoresistance (Hou et al., 2017; Liang et al., 2014; Wong et al., 2014). Histone deacetylase inhibitors have demonstrated promise in PDAC pre-clinical studies and are currently being investigated in multiple clinical trials (Feng et al., 2014). In agreement with these findings, over-expression of HDAC2 demonstrated resistance to oxaliplatin relative to control cells (Figure S10B), however our validation was likely limited by the level of HDAC2 over-expression achieved for this already highly expressed gene (Figure S6B).

CRISPR screen data can be used globally to predict chemosensitivity

Our screen yielded a large number of candidate genes and the validation of top hits suggests that our results are rich with new genes relevant to drug resistance. Since it is not feasible to individually validate all interesting genes, we sought to globally validate data from our screen. We reasoned that if our screen represents a gene's ability to confer drug resistance, then expression of genes that were top hits in our screens could be used to predict drug sensitivity in cell lines. To test this, we summed the product of a cell line's scaled expression data and the square of the L2FC sum for a given drug for each gene to generate a putative resistance score (Figure 4A). This method was tested on two independent previously published data sets characterizing PDAC cell line drug sensitivity. We found our predicted drug response scores significantly associated with observed irinotecan and gemcitabine sensitivity in the 18 pancreatic cancer lines assayed by cancer cell line encyclopedia (Barretina et al., 2012) and 14 lines from our own published work (Figure 4B-C, Kirby et al., 2017). Our drug response predictions were also able to respond to dynamic changes within a cell type. An increase in

predicted drug resistance was observed in each of seven PDAC cell lines after a weeklong treatment with a sub lethal dose of gemcitabine (Figure 4D). Finally, we assessed the performance our gemcitabine resistance predictions in patients who received adjuvant gemcitabine chemotherapy, but found our predictions were only meaningful for patients at the extreme ends of predicted sensitivity or resistance (Figure 4E).

DISCUSSION

The ability to both inhibit and endogenously activate the expression of genes in a modular and programmable manner has revolutionized forward genetic screening and is empowering discoveries that were previously impossible (Gersbach and Barrangou, 2018). We present the largest screen for cellular mechanisms of chemoresistance in PDAC cells to date and the first screen to perform both genome-wide knock out and endogenous activation in PDAC cells. The scale of our screen has allowed us to make a few fundamental observations of CRISPR screening that may be generalizable outside of PDAC. First, we found that the selection strength was the methodological variable most significantly correlated with our screen reproducibility. The implication of this finding is that the false positive rate of a screen is likely to be dose dependent and investigators should make every effort to perform as strong of a selection as possible. This can be difficult to achieve in screens incorporating cytotoxic chemotherapies such as ours because cells often accumulate damage throughout an extended selection period and will exhibit residual death after the drug is removed from the media. Thus, significant effort should be made to ensure appropriate selection strength, which in our hands was roughly 80% selection relative to control cells, while maintaining sufficient survivorship for sequencing library construction post-selection.

The second general observation was a relatively weak correlation between replicate reproducibility and gene significance levels across cell lines. While this observation may be partially explained by methodological covariates like selection strength (Figure S4), it is also likely that strong genetic and phenotypic differences observed between these cell lines (Kim et al., 2014) permit different mechanisms of chemoresistance. A gene capable of modulating chemosensitivity across every PDAC cell line would be an ideal target, however, our data suggests that this is not a realistic expectation. Previous screens for chemoresistance in PDAC cell lines have been limited in that they only use one cell line (Bhattacharjee et al., 2014; You et al., 2011) and our study is likely undersampling the natural variation in PDAC with only two cell lines. As sequencing and screening costs decrease, future studies examining orders of magnitude greater numbers of cell lines will likely add to the knowledge catalogued by our study.

Our last general observation is that genes and pathways associated drug-specific resistance tended to be less associated with PDAC patient survival than multi-drug resistance pathways. This result mirrors the reality of current PDAC clinical management in which patients are routinely treated with multiple drugs as frontline therapy (Garrido-Laguna and Hidalgo, 2015) and, at least at the cellular level, drug-specific mechanisms of resistance likely account for a smaller proportion of chemoresistance. As the rational design and delivery of multi-drug cocktails becomes more sophisticated and widely used we expect this observation to be made in other cancers as well (Hu et al., 2016).

We found *ABCG2* to be the most consistent gene associated with resistance across each drug and both cell lines. *ABCG2* is a well-described gene capable of mediating multi-drug resistance and as a efflux pump capable of acting upon a broad range of substrates, the mechanism of resistance is clear and helps to confirm the validity of our findings. Our validation

data confirm that two independent guides confer resistance to multiple drugs in multiple cell lines. However, we were unable to find evidence of *ABCG2* expression being correlated with patient survival in PDAC patients, thus the clinical relevance is unknown, however some evidence suggests that *ABCG2* expression is localized to cancer stem cells, which represent a minority of the total cell population, thus *ABCG2*'s role may be obscured from bulk tumor sequencing (Bhagwandin et al., 2016). It is for that reason we sought to demonstrate that inhibition of ABCG2 has the potential to sensitize cells to cytotoxic chemotherapy. Our findings suggest that further investigation of these agents would be warranted.

We also identified several components of the hemidesmisome complex as capable of mediating multi-drug resistance and possessing a strong correlation with patient survival across multiple cohorts. The hemidesmisome is critical for cells to adhere to the basement membrane and has been described as a core regulator of cell adhesion-mediated drug resistance (CAM-DR)(Correia and Bissell, 2012). CAM-DR is increasingly recognized for its importance in PDAC and the evolutionary trade offs between cells committing to epithelial-to-mesenchymal transition (EMT) in favor of metastasis as opposed to maintaining connections to the basement membrane and engaging in CAM-DR is an active area of investigation(Makohon-Moore and Iacobuzio-Donahue, 2016). As expression of hemidesmisome genes are strongly associated with quasi-mesenchymal/squamous subtype, genes identified by this study represent candidate markers and drivers of the poor patient prognosis described with this subtype across multiple studies (Bailey et al., 2016; Collisson et al., 2011; Moffitt et al., 2015; Raphael et al., 2017). While the hemidesmisome is not readily targetable, the quasi-mesenchymal/squamous subtype has been previously characterized as sensitive to the *EGFR* inhibitor, erlotinib. Erlotinib was approved for PDAC despite marginal survival benefits and its widespread use has been limited

by lack of a reliable biomarker capable of identifying responsive patients (Garrido-Laguna and Hidalgo, 2015). Performing tumor RNA-sequencing to cluster tumors into corresponding subtypes, which often have fluid definitions across studies, may be difficult clinically, however measuring a few components of the hemidesmisome complex identified by our study, such as *PLEC,* may be clinically tractable.

We also identified several transcriptional repressors including *REST,* the NCoR complex, and the NuRD complex as important regulators of chemosensitivity. Previous complementary studies have found recurrent inactivating mutations in several transcriptional activators including the SWI/SNF complex and the histone methyltransferases *MLL2* and *MLL3* in PDAC patients (Ryan et al., 2014). The transcriptional repressors identified by our study, such as *HDAC2,* are responsible for broad epigenetic reprogramming, thus future investigations will involve narrowing down the key epigenetic changes linked to resistance.

Lastly, we used our CRISPRa data to generate an algorithm for predicting sensitivity to drugs assayed in our study. We provided evidence of our algorithm's performance for gemcitabine and irinotecan in two independent studies that cataloged drug sensitivity and transcription of several PDAC cell lines. Our algorithm performed less well in predicting the survival PDAC patients treated with gemcitabine, only holding predictive power at the extreme ends of sensitivity prediction. This is likely explained by multiple non-cellular factors contributing to patient survival, such as comorbidities, patient drug metabolism, immune response, and stage at diagnosis. Thus cellular mechanisms of resistance may only dictate patient response in outlier cases. Furthermore, the expression data used to predict patient response was obtained from treatment naïve tumors and tumor sensitivity profiles may change at disease recurrence. We hope this effort inspires further attempts to integrate screening data with

transcriptional profiling to predict drug response and facilitate rational combination chemotherapy.

ACKNOWLEDGEMENTS

We thank the Myers and Cooper labs for helpful feedback. We also thank the HudsonAlpha genome services laboratory for assistance and optimizing the sequencing parameters of our CRIPSR screen. We also acknowledge The Cancer Genome Atlas, Cancer Cell Line Encyclopedia project datasets, which were extremely valuable and without which this study would not be possible. This work was supported by the State Cancer Fund of Alabama (to RMM). RCR and AAH were funded by the UAB MSTP (NIH-NIGMS 5T32GM008361-21. SJC and ERG were supported by the HudsonAlpha Tie the Ribbons Fund. SJC received support from the UAB CCTS grant (NIH 1UL1TR001417-01) and the UAB Comprehensive Cancer Center (NIH 5P30CA013148).

CONTRIBUTIONS

RCR, AAH, SJC and SJC designed the experiments. RCR, AAH, and ERG collected data. RCR, AAH, and ERG analyzed the data. RCR, AAH, and SJC wrote the first draft. All authors contributed to writing of the paper and read and approved the final manuscript.

DECLARATION OF INTERESTS

The authors report no conflicts.

FIGURE LEGENDS

Figure 1. CRISPR screen reveals drug resistance genes. (A) Schematic describing our screening protocol. (B) A heatmap of the sgRNA count per million, z-scored by row for the most variable 500 sgRNAs across all of our CRISPRa screen replicates in the PANC-1 cell line. (C) A density plot shows enrichment across all resistance screens for each gene, measured by the mean log2 fold change over background and the gene's association with survival, -log10(p-value).

Figure 2. (A) A scatterplot shows the mean L2FC sum for all four drugs assayed in each of two cell lines. Inset displays a zoomed out view of the entire plot. (B) Boxplots indicate the sgRNA fold change in counts per million comparing treated cells to control cells for each replicate and each cell line for the top *ABCG2* sgRNA. (C) Barplots indicating the mean *ABCG2* expression post sgRNA treatment as assayed by RNA-sequencing for two guides targeting ABCG2 (ABCG2_A and ABCG2_B) compared to two non-targeting controls (NTC1, NTC2). (D) Survival curves displaying the fraction of cells surviving a series of oxaliplatin doses for cells stable expressing an *ABCG2*-targeting sgRNA (blue) or non-targeting control sgRNAs (red and black). E) In ABCG2 over-expressing cells, we measured cell survival compared to cells with a non-targeting control guide under the indicated drug treatments. Plot indicates fold-change in survival compared to NTC2 with no inhibitor (blue), 3 uM sorafenib (green), and KO143 (maroon).

Figure 3. (A) For each pathway, an individual box represents an enrichment p-value for each of three guides targeting genes in the indicated pathway. (B) Scatter plot showing pathways enriched for multi-drug resistance in our CRISPRa and CRISPRko screens and their association with patient survival in the TCGA cohort. Patient survival is represented by the size and color of the circle. (C) Barplot indicating the percentile rank of the most enriched sgRNA targeting each

member of the hemidesmisome assembly pathway (Reactome). (D) Survival curves displaying the fraction of Panc-1 cells surviving a series of oxaliplatin doses for cells stable expressing a *PLEC*-targeting sgRNA (blue) or non-targeting control sgRNAs (red/black). (E) Boxplots displaying the mean expression level of members of the hemidesmisome assembly pathway in each of the subtypes described by Bailey et. al. (F) Boxplots indicating the mean expression level of hemidesmisome assembly pathway members in Kirby et. al patients surviving <300 days or >900 days and ICGC patients surviving <300 days or >900 days.

Figure 4. (A) Schematic describing the algorithm for predicting drug response from transcriptome data. A matrix of Z-scored gene expression for all genes across all samples, weighted by a vector corresponding to each gene's measured association with resistance to the drug in the screen. (B) Scatterplot showing observed irinotecan IC50 values compared to predicted sensitivity for 18 PDAC cells assayed by the Cancer Cell Line Encyclopedia. Rho=0.44, p-0.06. (C) Predicted gemcitabine sensitivity plotted compared to observed IC50 group for 15 PDAC cell lines assayed by Kirby et al. Wilcoxon Rank sum p=0.09. (D) Kaplan-Meier plot showing the change in predicted sensitivity before and after treatment with a sub-lethal dose of gemcitabine in several PDAC cell lines. Chi-squared p=0.01 (E) Boxplots indicating the survival time of PDAC patients treated with gemcitabine stratified by their predicted gemcitabine sensitivity of treatment naïve, resected tumor.

STAR METHODS

Contact for Reagent and Resource Sharing

Further information and requests for resources and reagents should be directed to and will be fulfilled by the Lead Contact, Sara Cooper (sjcooper@hudsonalpha.org).

Experimental Model and Subject Details

Cell culture

Panc-1 (CRL-1469), BxPC3 (CRL-1687), and MiaPaca-2 (CRL-1420) cell lines were obtained from ATCC. All cell lines were maintained in DMEM (ThermoFisher #11965) supplemented with 10% FBS (VWR #16777), 0.5% Penicillin-Streptomycin (ThermoFisher #15140122), and 0.5% GlutaMAX (ThermoFisher #A12860). All cell lines were maintained at 37°C and 5% CO_2.

Method Details

Plasmids

LentiCas9-Blast (Addgene #52962) was used to generate cell lines stably expressing CAS9 for knock out screening. Lenti-dCAS9-VP46-Blast (Addgene #61425) and lenti-MS2-p65-HSF1-Hygro (Addgene #61426) were used to generate cells for gene activation. The GeCKO A pooled sgRNA library (Addgene #1000000049) was used for gene knock out screening and the SAM pooled sgRNA library (Addgene #1000000057) was used for gene activation screening. LentiCrispr-v2 (Addgene #52961) was used for single gene knock out validation and lentiSAMv2 (Addgene #75112) was used for single gene activation validation. Guides were cloned as described previously (Joung et al., 2017). pMD2.G (Addgene #12259) and psPAX2 (Addgene # 12260) were used to facilitate viral packaging of sgRNA pools and single vector plasmids.

Library amplification

The GeCKO A and SAM library were amplified as described previously (Joung et al., 2017). Briefly, for each pooled library 8 electroporations were performed using 1uL of library and 25uL of Lucigen Endura Electrocompetent cells (Lucigen #60242). Electroporations were recovered in 1.975mLs of recovery media and rotated at 250 rpm for 1hr at 37°C. All electroporations were pooled after incubation and 2mLs of transformation were plated on 8-25cm^{2} bioassay plates with LB agar containing ampicillin. Plates were grown for 14hrs at 35°C. Transformation efficiency was greater than 1x10^{8} for both libraries. Bacterial colonies were scraped off of bioassay plates in 20mL of LB broth, pelleted and stored at -20°C for less than 1 week. Plasmid DNA was extracted from greater than 3g of pellet using the Qiagen EndoFree Plasmid Maxi Kit (Qiagen #12362).

Viral packaging

HEK 293FT cells (ThermoFisher #70007) were cultured in DMEM (ThermoFisher #11965) supplemented with 10% FBS (VWR #16777), 0.5% Penicillin-Streptomycin (ThermoFisher #15140122), 0.5% Non-essential amino acids (ThermoFisher #11140), and 0.5% sodium pyruvate (ThermoFisher #11360070). Viral packaging of pooled sgRNA libraries was performed in three 225cm^{2} flasks. One hour prior to transfections, after cells had reached ~60% confluency, DMEM was removed and replaced with 13mL of pre-warmed OptiMEM (ThermoFisher #31985). For each 225cm^{2} flask, 15.3ug of pMD2.G, 23.4ug psPAX2, and 30.6ug of pooled library were combined with 200uL of Lipofectamine PLUS reagent (ThermoFisher #15338) in 4mL of OptiMEM and vortexed to mix. Separately, 100uL of Lipofectamine LTX (ThermoFisher #15338) was diluted in 4mL of OptiMEM, vortexed, and incubated at room temperature for 5 minutes. The lipofectamine and plasmid solutions were then combined,

vortexed, and incubated for 5 additional minutes at room temperature. The 8mLs of combined solution were added to each flask. After incubating for 6 hours, PptiMEM was replaced with the original DMEM culture media supplemented with 1% bovine serum albumin (ThermoFisher #A9647). After 60 hours, the media was harvested, centrifuged at 3000rpm for 10 minutes at 4°C, filtered through a 0.45um filter (VWR #28145), and stored at 4°C overnight in Lenti-X concentrator (Clontech #631231) at a 3:1 virus to Lenti-X concentrator volume ratio. The following day the virus was centrifuged at 1,500g for 45 minutes at 4°C and the supernatant was poured off. The viral pellet was resuspended in DMEM culture media at one-tenth the original volume and stored at -80°C. Packaging of other vectors was performed identically to the pooled library, with reagents scaled down proportionally according to the surface area of the appropriate flask.

Viral packaging of single sgRNAs used for validation was performed in 6-well tissue culture treated plates. The day prior to transfection, 750,000 HEK293T cells were seeded into a 6 well plate; minimum one well per sgRNA. One hour prior to transfections, after cells had reached ~90% confluency, DMEM was removed and replaced with 3mL of pre-warmed OptiMEM (ThermoFisher #31985). For each well to be transfected, 1ug of pMD2.G and 1.5ug psPAX2 were combined with 12.5uL of Lipofectamine 2000 reagent (ThermoFisher #11668019) in 200uL of OptiMEM and vortexed to mix. Separately, 10uL of Lipofectamine PLUS reagent (ThermoFisher #15338) was diluted in 200 uL of OptiMEM and vortexed to mix. Both master mixes are combined and added to a tube containing 2.5ug of sgRNA plasmid, vortexed, and incubated at room temperature for 5 minutes. The 400uL of combined solution were added to each corresponding well in the 6-well late. After incubating for 48 hours, the media was

harvested, centrifuged at 3000rpm for 10 minutes at 4°C, filtered through a 0.45um filter (VWR #28145). Virus was either immediately stored at -80°C or used for transfection.

Drug resistance screening

Panc-1 and BxPC3 cell lines were transduced with LentiCas9-Blast or co-transduced with Lenti-dCAS9-VP46-Blast and lenti-MS2-p65-HSF1-Hygro for knock out and activation screening respectively. 500,000 cells were seeded into each well of a six-well flask with 0.8ug/mL polybrene (Sigma #TR-1003-G). Previously packaged plasmid added at volumes that ranged from 0 to 500uL of virus. Cells were then centrifuged at 2000rpm for 2 hours at 37°C. After centrifugation the cells were incubated overnight and media was changed the following morning. The following day cells were treated with appropriate antibiotic. Panc-1 cells were treated 10ug/mL Blasticidin and 1500ug/mL Hygromycin and BxPC3 cells were treated with 2.5ug/mL Blasticidin and 1250ug/mL Hygromycin. Cells were kept under antibiotic selection for one week post-transduction until no-virus control cells were dead. The lowest viral titer that had a sufficient number of cells to carry forward were grown up such that pooled libraries could be transduced at 500x representation at a multiplicity of infection (MOI) of 0.4:

Min. cells needed = 70,000 sgRNAs x 500 cells/sgRNA x (1/0.4) = 87.5x10^{6} cells

Pooled library transduction was performed in at least 30 wells of a 12 well flask at 3x10^{6} cells per well with 0.8ug/mL polybrene and sufficient volume of concentrated virus to reach an MOI of 0.4 (approximately 30% of cells surviving after antibiotic selection). Cells were transduced as described above. The following day cells were split out into larger 225cm^{2} flasks and either puromycin (Panc-1 10ug/mL, BxPC3 2.5ug/uL) or zeocin (Panc-1 2mg/mL, BxPC3 3mg/mL) was added to select for presence of knock out and activation plasmids, respectively. Library-transduced cells were under selection for one week post-transduction and expanded to

$7x10^7$ cells per treatment replicate or 1000x representation for each of the 4 drug and control conditions per replicate. A minimum 500x representation was maintained at all times in control cells. Drug treatments included gemcitabine (Tocris #G6423, Panc-1 25nM, BxPC3 25nM), oxaliplatin (Sigma #O9512, Panc-1 2.5uM, BxPC3 2.5uM), irinotecan (Sigma #I1406, Panc-1 500nM, BxPC3 250nM), and 5-fluorouracil (Sigma #F6627, Panc1 7.5uM, BxPC3 5uM). All doses were optimized to yield ~20% the number of viable cells in drug treated cells relative to untreated control cells after 14 days of culture. After 14 days of drug treatment, cells were counted, pelleted, and stored at -80°C. The first replicate of the knock out screen for each cell line was performed separately from the second two in order to optimize all drug doses and library preparation methods. All three replicates of the activation screen were performed in parallel for each cell line.

DNA extraction and library preparation

Genomic DNA was extracted from cell pellets adapting a previously published protocol (Chen et al., 2015). The protocol described below assumes $5x10^7$ input cells, but can be scaled proportionally to accommodate different cell ranges. Briefly, cells were resuspended in 6mLs of a NK lysis buffer (50mM Tris (ThermoFisher #BP1757)), 50mM EDTA (Fluka #03690), 1% SDS (Invitrogen #15525), and 30uL of 20mg/mL Proteinase K (Zymogen #D3001)) and incubated at 55°C overnight. The following morning, 30uL of 10mg/mL RNAse A (Qiagen 19101) was added to the lysate, inverted several times, and incubated at 37°C for 30 minutes. Next, 2mL of chilled 7.5M ammonium acetate (ThermoFisher #631-61-8) was added to the lysate, vortexed for 20 seconds, and centrifuged at 4100xg for 10 minutes at room temperature. The supernatant was carefully decanted to a fresh conical tube and 6mLs of 100% isoproponal (Sigma #I9516) was added to the tube inverted 50 times and centrifuged at 4100xg for 10

minutes. The supernatant was then discarded, 6mLs of 70% ethanol (Sigma #E7023) was added to the DNA pellet, and centrifuged at 4100xg for 1 minute after inverted 10 times. The supernatant was pipetted off carefully and the DNA pellet was dried at room temperature for 1 hour. 500uL of TE buffer (Sigma #T9285) was added to the dried pellet and the tube was incubated at 65°C 1-2 hours. Next the conical tubes were briefly spun at 1000xg to pull down any evaporated TE buffer and incubated for 2-3 days at room temperature vortexing periodically. If necessary, additional TE buffer was added until the DNA pellet was completely dissolved. The gDNA concentration was measured using Qubit fluorometric quantitation (ThermoFisher #Q32850).

Two-step PCR reactions were used to amplify and append sequencing tails to both the activation and knock out libraries. Primer sequences are available in Table S5. To maintain 500x representation in control samples we performed 86 50uL PCR1 reactions (or as many reactions as possible for drug selected samples) per replicate each containing 2.5ug gDNA, 2.5 uL of appropriate forward and reverse primer (25uM), 25uL NEBNext High-Fidelity 2X PCR master mix (NEB #M0541), and the remaining volume required to reach 50uL in nuclease-free water. For the knock out library, we performed an initial denaturation of 98°C for 60 seconds, 18 cycles of 98°C denaturation for 15 seconds, 62°C annealing for 30 seconds, 72°C extension for 30 seconds, a final extension of 72°C for 5 minutes, and a 4°C hold. The activation screen PCR1 was carried out under identical conditions except the annealing temperature was adjusted to 60°C and only 16 cycles of PCR were performed. PCR1 reactions for each replicate of each treatment condition were pooled and the second PCR reaction (PCR2) was used to append Illumina sequencing tails.

We performed 12 PCR2 reactions for each replicate of each condition consisting of 2.5uL of pooled PCR1, 2.5uL of appropriate forward and reverse primer (10uM), 25uL NEBNext High-Fidelity 2X PCR master mix, and 20uL of nuclease-free water. The PCR conditions were carried out similarly to PCR1 except it was reduced to 10 cycles for each reaction with an annealing temperature of 65°C for the knock library amplification and 69°C for the activation library amplification. All PCR2 reactions for each replicate of each condition were pooled and 50uL was run on a 2% gel at 125V for 2 hours. A 240bp or 280bp band for the knock out or activation library respectively was excised and gel extracted (Qiagen #28704). All controls and drug treated samples for each replicate were prepped in the same batch in order to avoid batch affects.

Single gene validation

The top sgRNAs for genes of interest were cloned into either LentiCrispr-v2 or LentiSAMv2 for knock out or activation screen validation as described previously (Konermann et al., 2015). (Sequences are available in Table S6). Plasmids putatively containing sgRNAs of interest were transformed into One Shot Stbl3 competent *E. coli* (ThermoFisher #C737303). Colonies that survived ampicillin selection were cultured overnight in 10mL of LB broth containing ampicillin. Plasmids were harvested with an E.Z.N.A Endo Free plasmid mini kit (Omega #D6950) and confirmed to contain the appropriate sgRNA with Sanger sequencing. To generate stable cell lines expressing each sgRNA, single sgRNA plasmids underwent viral packaging and were transduced as described previously, followed by transduction. For transduction 10^6 cells were seeded per well of a 6-well plate for a total volume of 2mL of cells and media. To that we added, 1.6ul of polybrene (Millipore Sigma #TR-1003-G), and 1mL of

packaged virus. Then, we used spinfection for 30 minutes at 2000RPM at 37C. All lines were established using antibiotic selection as described above.

Non-targeting and targeting sgRNAs were plated in 96-well plates at 750 cells/well and treated with a range of gemcitabine, oxaliplatin, or irinotecan concentrations. Plated cells were grown for 6 and 8 days, for the knockout and activation screen, respectively, with the media changed and drug applied every 2 days. The number of viable cells surviving drug treatment was assayed with Cell Titer-Glo cell (Promega #G7571). ABCG2 inhibition was done under these conditions as well, with the only change being the addition of 3uM Sorafenib or 3uM KO143 where indicated. Two NTCs were tested and the complete data sets is available in Figure S11.

RNA-sequencing

RNA was extracted from cell pellets containing 3 x 10^5 cells. Cells were suspended in 400 ul of RL Buffer from the Norgen total RNA extraction kit (cat. # 37500, 25720) plus 1% BME. Samples were homogenized by vortex. We then continued extraction of RNA with the Norgen Total RNA extraction kit including the Norgen DNase kit (cat. # 37500, 25720). RNA integrity numbers (RIN) were measured using the BioAnalyzer (Agilent) and all measured at a RIN of 10 indicating high quality RNA. RNA was quantified using Qubit 2.0 Fluorometer (Thermofisher). We used 1000 ng of total RNA as input to the NEBNext Poly(A) mRNA Magnetic Isolation Module (NEB cat# E7490S) followed by the NEBNext Ultra RNA Library Prep Kit for Illumina (cat# E7530S). Libraries were barcoded using the Genomic Services Lab at HudsonAlpha's custom dual index barcode plate. We pooled all samples onto a lane of a S4 NovaSeq flow cell, and sequenced an average of 95.8 million 150bp paired-end reads per sample with an average Q30 score of 95%. Samples were processed using our published primary analysis tool, aRNApipe (Alonso et al., 2017).

Quantification and Statistical Analysis

Sequencing and data processing

Three sets of replicates (control and 4 drug treated samples) for each cell line were sequenced on one lane of Illumina NextSeq resulting in an average of 40 million reads per sample. 5' and 3' adapters were observed in >99% of reads and were trimmed using cutadapt (Martin, 2011). Adapter trimmed fastq files were then aligned to the gRNA libraries and raw count tables generated using MAGeCK (Li et al., 2014). We had a perfect alignment rate of 72%-74% of raw reads for each sample. Sequencing the control samples revealed sufficient representation of guides with an average of 99.8% and 99.3% of sgRNAs detected and 98.4% and 94.2% of sgRNAs detected at greater than 1 read per million in our knock out and activation control samples, respectively. A $\log_2$ fold change was computed for each sgRNA in each drug treated sample relative to the untreated control sample for each replicate. sgRNAs with less than 10 counts in the untreated control samples and less than 50 counts in a treated control sample were excluded from further analysis (<1% of sgRNAs)(Table S1A-B). At this step we recognized the first replicate of our knock out screen correlated relatively poorly with the second two replicates and was excluded from downstream analysis. We ranked each of the sgRNAs targeting each gene by the minimum $\log_2$ fold change across each replicate. Top genes were subsequently prioritized for follow up by their "L2FC sum" in each cell line, which is the sum of the replicate minimum $\log_2$ fold changes of the top two sgRNAs targeting each gene. Multi-drug hits were prioritized by computing the mean "L2FC sum" across each of the four drug treatments. Pathways enriched for genes conferring drug resistance were identified by comparing the distribution of $\log_2$ fold changes for the top, second, and third sgRNA targeting each gene within a Reactome pathway to that of all other genes by Wilcox ranked sum test. Reactome

(Fabregat et al., 2018) pathways with fewer than 10 genes targeted in our libraries were excluded. A consolidated knock out and activation score was computed for each pathway by summing the $-\log_{10}$ P-values for the top, second, and third sgRNAs of each pathway (Table S4).

Curve fitting single gene validation

Where EC50 values were calculated, we use cell count data as measured by Cell Titer Glo, as input, and fit those data to a rectangular hyperbola which led to the use of we used Michaelis-Menten equation to curve fit the data and derive the estimated drug concentration at which the drug is half its maximum effectiveness and confidence intervals for each cell line, drug, and guide combination. We used those data to determine the change in EC50 and p-value associated with those changes for each guide compared to each of the two non-targeting controls (NTCs) . These calculations were done using Prism GraphPad 7.

Predicting drug response using genome-wide screening results

Sensitivity to each of the four drugs was computed using a cell line's treatment naïve gene expression levels and the minimum L2FC Sum for each gene across both cell lines. Raw expression data for each cell line, obtained from sources described below, was processed into raw count tables using the aRNApipe RNA-seq processing pipeline (Alonso et al., 2017). Cell line gene expression data was normalized using the R package DESeq2's variance stabilizing transformation (Love et al., 2014) and each gene's expression level was z-scored across each cell line. Next, a scalar by which to weight each gene's expression level was computed using the L2FC Sum described above. The replicate minimum L2FC sum from the relevant drug's CRISPRa screen was used for all genes who's L2FC Sum was greater than 0. The replicate maximum L2FC sum was used for all genes whose L2FC Sum was less than 0. All other genes were assigned a scalar value of zero. The L2FC Sum scalar was squared to ensure a positive

value and place more weight on genes with high absolute fold change. Next, the product of each gene's z-scored expression data and L2FC Sum scalar was computed to generate a weighted expression value for each gene. Finally, the cumulative sum of the weighted expression value for each gene with a negative L2FC Sum in each cell line was subtracted from the cumulative sum of the weighted expression value for each gene with a positive L2FC Sum to generate a single value representing a cell line's expected level of resistance to the given drug. Irinotecan sensitivity and gene expression data were obtained for 18 PDAC cell lines with permission from the Cancer Cell Line Encyclopedia (Barretina et al., 2012) (https://portals.broadinstitute.org/ccle). Gemcitabine sensitivity (cell lines were classified as sensitive, intermediate, or resistant) and gene expression data for 14 PDAC cell lines was obtained from previously published work (Kirby et al., 2016). A panel of five PDAC cell lines was screened for oxaliplatin sensitivity by treating with serial dilutions of the drug as described previously (Kirby et al., 2016). Cell counts at each dose were compared to a vehicle control to construct a six-point dose response curve. The area under the dose-response curve was used to compare sensitivity. Patient expression data and treatment info was obtained from a previous study at the GEO accession GSE79670.

Data and Software Availability

Data generated by this study have been made available through public databases. Screening data are available at SRA by referencing the BioProject number PRJNA542321. RNA-sequencing data are available at GEO using the accession GSE131596.

Key Resources Table

Reagent or Resource	Source	Identifier
Bacterial and Virus Strains		
Lucigen Endura Electocompetent Cells	Lucigen	#60242
Chemicals		
Sorafenib	Cayman Chemicals	#10009644
KO143	Cruz Chem	sc-204030A
Deposited Data		
RNA-sequencing	This paper	GSE131596
CRISPR Screening sgRNA amplicon sequencing	This paper	PRJNA542321
RNA-sequencing of pancreatic cancer cell lines	Kirby et al 2016	GSE79670
Experimental Models: Cell Lines		
HEK 293 FT	ThermoFisher	#70007
Panc-1	ATCC	CRL-1469
BxPC3	ATCC	CRL-1687
MiaPaca-2	ATCC	CRL1420
Oligonucleotides		
See Supplemental Tables	Integrated DNA Technologies	NA
Recombinant DNA		
LentiCas9-Blast	AddGene	#52962
Lenti-dCas9-VP46-Blast	AddGene	#61425
Lenti-MS2-p65-HSF1-Hygro	AddGene	#61426
GeckoA pooled sgRNA library	AddGene	#1000000049
SAM pooled sgRNA library	AddGene	#1000000057
LentiSAMv2	AddGene	#75112
pMD2.G	AddGene	#12259

psPAX2	AddGene	#12260
Software and Algorithms		
aRNA-pipe	Alonso et al 2017	https://github.com/HudsonAlpha/aRNAPipe
MaGeCK	Li et al 2014	http://liulab.dfci.harvard.edu/Mageck/

REFERENCES

Allen, J.D., Loevezijn, A. Van, Lakhai, J.M., Valk, M. Van Der, Tellingen, O. Van, Reid, G., Schellens, J.H.M., Koomen, G., and Schinkel, A.H. (2002). Potent and Specific Inhibition of the Breast Cancer Resistance Protein Multidrug Transporter in Vitro and in Mouse Intestine by a Novel Analogue of Fumitremorgin C 1. *1*, 417–425.

Alonso, A., Lasseigne, B.N., Williams, K., Nielsen, J., Ramaker, R.C., Hardigan, A.A., Johnston, B.E., Roberts, B.S., Cooper, S.J., Marsal, S., et al. (2017). aRNApipe: A balanced, efficient and distributed pipeline for processing RNA-seq data in high performance computing environments. Bioinformatics *11*, 1727–1729.

Bailey, P., Chang, D.K., Nones, K., Johns, A.L., Patch, A.-M., Gingras, M.-C., Miller, D.K., Christ, A.N., Bruxner, T.J.C., Quinn, M.C., et al. (2016). Genomic analyses identify molecular subtypes of pancreatic cancer. Nature *531*, 47–52.

Barretina, J., Caponigro, G., Stransky, N., Venkatesan, K., Margolin, A.A., Kim, S., Wilson, C.J., Lehár, J., Kryukov, G. V., Sonkin, D., et al. (2012). The Cancer Cell Line Encyclopedia enables predictive modelling of anticancer drug sensitivity. Nature *483*, 603–607.

Bazhin, A. V, Bayry, J., Umansky, V., Werner, J., and Karakhanova, S. (2013). Overcoming

immunosuppression as a new immunotherapeutic approach against pancreatic cancer. Oncoimmunology *2*, e25736.

Bhagwandin, V.J., Bishop, J.M., Wright, W.E., and Shay, J.W. (2016). The Metastatic Potential and Chemoresistance of Human Pancreatic Cancer Stem Cells. PLoS One *11*, e0148807.

Bhattacharjee, V., Zhou, Y., and Yen, T. (2014). A synthetic lethal screen identifies the Vitamin D receptor as a novel gemcitabine sensitizer in pancreatic cancer cells. Cell Cycle *13*, 3839–3856.

Bollag, G., Tsai, J., Zhang, J., Zhang, C., Ibrahim, P., Nolop, K., and Hirth, P. (2012). Vemurafenib: the first drug approved for BRAF-mutant cancer. Nat. Rev. Drug Discov. *11*, 873–886.

Chen, S., Sanjana, N.E., Zheng, K., Shalem, O., Lee, K., Shi, X., Scott, D.A., Song, J., Pan, J.Q., Weissleder, R., et al. (2015). Genome-wide CRISPR Screen in a Mouse Model of Tumor Growth and Metastasis. Cell *160*, 1246–1260.

Chu, G.C., Kimmelman, A.C., Hezel, A.F., and DePinho, R.A. (2007). Stromal biology of pancreatic cancer. J. Cell. Biochem. *101*, 887–907.

Collisson, E.A., Sadanandam, A., Olson, P., Gibb, W.J., Truitt, M., Gu, S., Cooc, J., Weinkle, J., Kim, G.E., Jakkula, L., et al. (2011). Subtypes of pancreatic ductal adenocarcinoma and their differing responses to therapy. Nat. Med. *17*, 500–503.

Conroy, T., Desseigne, F., Ychou, M., Bouché, O., Guimbaud, R., Bécouarn, Y., Adenis, A., Raoul, J.-L., Gourgou-Bourgade, S., de la Fouchardière, C., et al. (2011). FOLFIRINOX versus Gemcitabine for Metastatic Pancreatic Cancer. N. Engl. J. Med. *364*, 1817–1825.

Correia, A.L., and Bissell, M.J. (2012). The tumor microenvironment is a dominant force in multidrug resistance. Drug Resist. Updat. *15*, 39–49.

Evers, B., Jastrzebski, K., Heijmans, J.P.M., Grernrum, W., Beijersbergen, R.L., and Bernards, R. (2016). CRISPR knockout screening outperforms shRNA and CRISPRi in identifying essential genes. Nat. Biotechnol. *34*, 631–633.

Fabregat, A., Jupe, S., Matthews, L., Sidiropoulos, K., Gillespie, M., Garapati, P., Haw, R., Jassal, B., Korninger, F., May, B., et al. (2018). The Reactome Pathway Knowledgebase. Nucleic Acids Res. *46*, D649–D655.

Feng, W., Zhang, B., Cai, D., and Zou, X. (2014). Therapeutic potential of histone deacetylase inhibitors in pancreatic cancer. Cancer Lett. *347*, 183–190.

Garrido-Laguna, I., and Hidalgo, M. (2015). Pancreatic cancer: from state-of-the-art treatments to promising novel therapies. Nat. Rev. Clin. Oncol. *12*, 319–334.

Gersbach, C.A., and Barrangou, R. (2018). Pulling the genome in opposite directions to dissect gene networks. Genome Biol. *19*, 42.

Goldman, J.M., and Melo, J. V (2003). Chronic myeloid leukemia--advances in biology and new approaches to treatment. N. Engl. J. Med. *349*, 1451–1464.

Griffith, M., Miller, C.A., Griffith, O.L., Krysiak, K., Skidmore, Z.L., Ramu, A., Walker, J.R., Dang, H.X., Trani, L., Larson, D.E., et al. (2015). Optimizing Cancer Genome Sequencing and Analysis. Cell Syst. *1*, 210–223.

Hou, M.-F., Luo, C.-W., Chang, T.-M., Hung, W.-C., Chen, T.-Y., Tsai, Y.-L., Chai, C.-Y., and Pan, M.-R. (2017). The NuRD complex-mediated p21 suppression facilitates chemoresistance in BRCA-proficient breast cancer. Exp. Cell Res. *359*, 458–465.

Hu, Q., Sun, W., Wang, C., and Gu, Z. (2016). Recent advances of cocktail chemotherapy by combination drug delivery systems. Adv. Drug Deliv. Rev. *98*, 19–34.

Joung, J., Konermann, S., Gootenberg, J.S., Abudayyeh, O.O., Platt, R.J., Brigham, M.D.,

Sanjana, N.E., and Zhang, F. (2017). Genome-scale CRISPR-Cas9 knockout and transcriptional activation screening. Nat. Protoc. *12*, 828–863.

Kamisawa, T., Wood, L.D., Itoi, T., and Takaori, K. (2016). Pancreatic cancer. Lancet (London, England) *388*, 73–85.

Kandoth, C., McLellan, M.D., Vandin, F., Ye, K., Niu, B., Lu, C., Xie, M., Zhang, Q., McMichael, J.F., Wyczalkowski, M.A., et al. (2013). Mutational landscape and significance across 12 major cancer types. Nature *502*, 333–339.

Katzel, J.A., Fanucchi, M.P., and Li, Z. (2009). Recent advances of novel targeted therapy in non-small cell lung cancer. J. Hematol. Oncol. *2*, 2.

Kim, Y., Han, D., Min, H., Jin, J., Yi, E.C., and Kim, Y. (2014). Comparative proteomic profiling of pancreatic ductal adenocarcinoma cell lines. Mol. Cells *37*, 888–898.

Kirby, M.K., Ramaker, R.C., Gertz, J., Davis, N.S., Johnston, B.E., Oliver, P.G., Sexton, K.C., Greeno, E.W., Christein, J.D., Heslin, M.J., et al. (2016). RNA sequencing of pancreatic adenocarcinoma tumors yields novel expression patterns associated with long-term survival and reveals a role for ANGPTL4. Mol. Oncol. *10*.

Kirby, M.K., Ramaker, R.C., Roberts, B.S., Lasseigne, B.N., Gunther, D.S., Burwell, T.C., Davis, N.S., Gulzar, Z.G., Absher, D.M., Cooper, S.J., et al. (2017). Genome-wide DNA methylation measurements in prostate tissues uncovers novel prostate cancer diagnostic biomarkers and transcription factor binding patterns. BMC Cancer *17*.

Konermann, S., Brigham, M.D., Trevino, A.E., Joung, J., Abudayyeh, O.O., Barcena, C., Hsu, P.D., Habib, N., Gootenberg, J.S., Nishimasu, H., et al. (2015). Genome-scale transcriptional activation by an engineered CRISPR-Cas9 complex. Nature *517*, 583–588.

Koong, A.C., Mehta, V.K., Le, Q.T., Fisher, G.A., Terris, D.J., Brown, J.M., Bastidas, A.J., and

Vierra, M. (2000). Pancreatic tumors show high levels of hypoxia. Int. J. Radiat. Oncol. *48*, 919–922.

Li, W., Xu, H., Xiao, T., Cong, L., Love, M.I., Zhang, F., Irizarry, R.A., Liu, J.S., Brown, M., and Liu, X.S. (2014). MAGeCK enables robust identification of essential genes from genome-scale CRISPR/Cas9 knockout screens. Genome Biol. *15*, 554.

Liang, J., Tong, P., Zhao, W., Li, Y., Zhang, L., Xia, Y., and Yu, Y. (2014). The REST gene signature predicts drug sensitivity in neuroblastoma cell lines and is significantly associated with neuroblastoma tumor stage. Int. J. Mol. Sci. *15*, 11220–11233.

Love, M.I., Huber, W., and Anders, S. (2014). Moderated estimation of fold change and dispersion for RNA-seq data with DESeq2. Genome Biol. *15*, 550.

Makohon-Moore, A., and Iacobuzio-Donahue, C.A. (2016). Pancreatic cancer biology and genetics from an evolutionary perspective. Nat. Rev. Cancer *16*, 553–565.

Mao, L., Li, Y., Zhao, J., Li, Q., Yang, B., Wang, Y., Zhu, Z., Sun, H., and Zhai, Z. (2017). Transforming growth factor-β1 contributes to oxaliplatin resistance in colorectal cancer via epithelial to mesenchymal transition. Oncol. Lett. *14*, 647–654.

Martin, M. (2011). Cutadapt removes adapter sequences from high-throughput sequencing reads. EMBnet.journal *17*, 10.

McDonald, O.G., Li, X., Saunders, T., Tryggvadottir, R., Mentch, S.J., Warmoes, M.O., Word, A.E., Carrer, A., Salz, T.H., Natsume, S., et al. (2017). Epigenomic reprogramming during pancreatic cancer progression links anabolic glucose metabolism to distant metastasis. Nat. Genet. *49*, 367–376.

Meng, E., Hanna, A., Samant, R.S., and Shevde, L.A. (2015). The Impact of Hedgehog Signaling Pathway on DNA Repair Mechanisms in Human Cancer. Cancers (Basel). *7*, 1333–1348.

Miyake, M., Fujimoto, K., Anai, S., Ohnishi, S., Nakai, Y., Inoue, T., Matsumura, Y., Tomioka, A., Ikeda, T., Okajima, E., et al. (2010). Inhibition of heme oxygenase-1 enhances the cytotoxic effect of gemcitabine in urothelial cancer cells. Anticancer Res. *30*, 2145–2152.

Mo, W., and Zhang, J.-T. (2012). Human ABCG2: structure, function, and its role in multidrug resistance. Int. J. Biochem. Mol. Biol. *3*, 1–27.

Moffitt, R.A., Marayati, R., Flate, E.L., Volmar, K.E., Loeza, S.G.H., Hoadley, K.A., Rashid, N.U., Williams, L.A., Eaton, S.C., Chung, A.H., et al. (2015). Virtual microdissection identifies distinct tumor- and stroma-specific subtypes of pancreatic ductal adenocarcinoma. Nat. Genet. *47*, 1168–1178.

Morgens, D.W., Deans, R.M., Li, A., and Bassik, M.C. (2016). Systematic comparison of CRISPR/Cas9 and RNAi screens for essential genes. Nat. Biotechnol. *34*, 634–636.

Niwa, T., Saito, H., Imajoh-ohmi, S., Kaminishi, M., Seto, Y., Miki, Y., and Nakanishi, A. (2009). BRCA2 interacts with the cytoskeletal linker protein plectin to form a complex controlling centrosome localization. Cancer Sci. *100*, 2115–2125.

Pao, W., Miller, V., Zakowski, M., Doherty, J., Politi, K., Sarkaria, I., Singh, B., Heelan, R., Rusch, V., Fulton, L., et al. (2004). EGF receptor gene mutations are common in lung cancers from “never smokers” and are associated with sensitivity of tumors to gefitinib and erlotinib. Proc. Natl. Acad. Sci. U. S. A. *101*, 13306–13311.

Raphael, B.J., Hruban, R.H., Aguirre, A.J., Moffitt, R.A., Yeh, J.J., Stewart, C., Robertson, A.G., Cherniack, A.D., Gupta, M., Getz, G., et al. (2017). Integrated Genomic Characterization of Pancreatic Ductal Adenocarcinoma. Cancer Cell *32*, 185–203.e13.

Ryan, D.P., Hong, T.S., and Bardeesy, N. (2014). Pancreatic Adenocarcinoma. N Engl J Med *371*, 1039–1049.

Sanchez-Vega, F., Mina, M., Armenia, J., Chatila, W.K., Luna, A., La, K.C., Dimitriadoy, S., Liu, D.L., Kantheti, H.S., Saghafinia, S., et al. (2018). Oncogenic Signaling Pathways in The Cancer Genome Atlas. Cell *173*, 321–337.e10.

Shugang, X., Hongfa, Y., Jianpeng, L., Xu, Z., Jingqi, F., Xiangxiang, L., and Wei, L. (2016). Prognostic Value of SMAD4 in Pancreatic Cancer: A Meta-Analysis. Transl. Oncol. *9*, 1–7.

Siegel, R.L., Miller, K.D., and Jemal, A. (2018). Cancer statistics, 2018. CA. Cancer J. Clin. *68*, 7–30.

Smith, S.C., Petrova, A. V, Madden, M.Z., Wang, H., Pan, Y., Warren, M.D., Hardy, C.W., Liang, D., Liu, E.A., Robinson, M.H., et al. (2014). A gemcitabine sensitivity screen identifies a role for NEK9 in the replication stress response. Nucleic Acids Res. *42*, 11517–11527.

Stathis, A., and Moore, M.J. (2010). Advanced pancreatic carcinoma: current treatment and future challenges. Nat. Rev. Clin. Oncol. *7*, 163–172.

Steinhart, Z., Pavlovic, Z., Chandrashekhar, M., Hart, T., Wang, X., Zhang, X., Robitaille, M., Brown, K.R., Jaksani, S., Overmeer, R., et al. (2017). Genome-wide CRISPR screens reveal a Wnt–FZD5 signaling circuit as a druggable vulnerability of RNF43-mutant pancreatic tumors. Nat. Med. *23*, 60–68.

Sun, C., Wang, F.-J., Zhang, H.-G., Xu, X.-Z., Jia, R.-C., Yao, L., and Qiao, P.-F. (2017). miR-34a mediates oxaliplatin resistance of colorectal cancer cells by inhibiting macroautophagy via transforming growth factor-β/Smad4 pathway. World J. Gastroenterol. *23*, 1816–1827.

Sun, Y., Gu, M., Zhu, L., Liu, J., Xiong, Y., Wei, Y., and Li, F. (2016). Gemcitabine upregulates ABCG2/BCRP and modulates the intracellular pharmacokinetic profiles of bioluminescence in pancreatic cancer cells. Anticancer. Drugs *27*, 183–191.

Tadros, S., Shukla, S.K., King, R.J., Gunda, V., Vernucci, E., Abrego, J., Chaika, N. V, Yu, F.,

Lazenby, A.J., Berim, L., et al. (2017). De Novo Lipid Synthesis Facilitates Gemcitabine Resistance through Endoplasmic Reticulum Stress in Pancreatic Cancer. Cancer Res. *77*, 5503–5517.

Tripathi, K., Mani, C., Barnett, R., Nalluri, S., Bachaboina, L., Rocconi, R.P., Athar, M., Owen, L.B., and Palle, K. (2014). Gli1 Protein Regulates the S-phase Checkpoint in Tumor Cells via Bid Protein, and Its Inhibition Sensitizes to DNA Topoisomerase 1 Inhibitors. J. Biol. Chem. *289*, 31513–31525.

Walko, G., Castañón, M.J., and Wiche, G. (2015). Molecular architecture and function of the hemidesmosome. Cell Tissue Res. *360*, 529–544.

Wang, T., Wei, J.J., Sabatini, D.M., and Lander, E.S. (2014). Genetic Screens in Human Cells Using the CRISPR-Cas9 System. Science (80-.). *343*, 80–84.

Warr, M.R., and Shore, G.C. (2008). Small-molecule Bcl-2 antagonists as targeted therapy in oncology. Curr. Oncol. *15*, 256–261.

Wei, Y., Ma, Y., Zhao, Q., Ren, Z., Li, Y., Hou, T., and Peng, H. (2012). New Use for an Old Drug: Inhibiting ABCG2 with Sorafenib. Mol. Cancer Ther. *11*, 1693–1702.

Witkiewicz, A.K., McMillan, E.A., Balaji, U., Baek, G., Lin, W.-C., Mansour, J., Mollaee, M., Wagner, K.-U., Koduru, P., Yopp, A., et al. (2015). Whole-exome sequencing of pancreatic cancer defines genetic diversity and therapeutic targets. Nat. Commun. *6*, 6744.

Wong, M.M., Guo, C., and Zhang, J. (2014). Nuclear receptor corepressor complexes in cancer: mechanism, function and regulation. Am. J. Clin. Exp. Urol. *2*, 169–187.

Yachida, S., and Iacobuzio-Donahue, C.A. (2009). The Pathology and Genetics of Metastatic Pancreatic Cancer. Arch Pathol Lab Med—Vol *133*.

You, L., Chang, D., Du, H.-Z., and Zhao, Y.-P. (2011). Genome-wide screen identifies PVT1 as

a regulator of Gemcitabine sensitivity in human pancreatic cancer cells. Biochem. Biophys. Res. Commun. *407*, 1–6.

Zhang, T., Yang, P., Wei, J., Li, W., Zhong, J., Chen, H., and Cao, J. (2018). Overexpression of flavin-containing monooxygenase 5 predicts poor prognosis in patients with colorectal cancer. Oncol. Lett. *15*, 3923–3927.

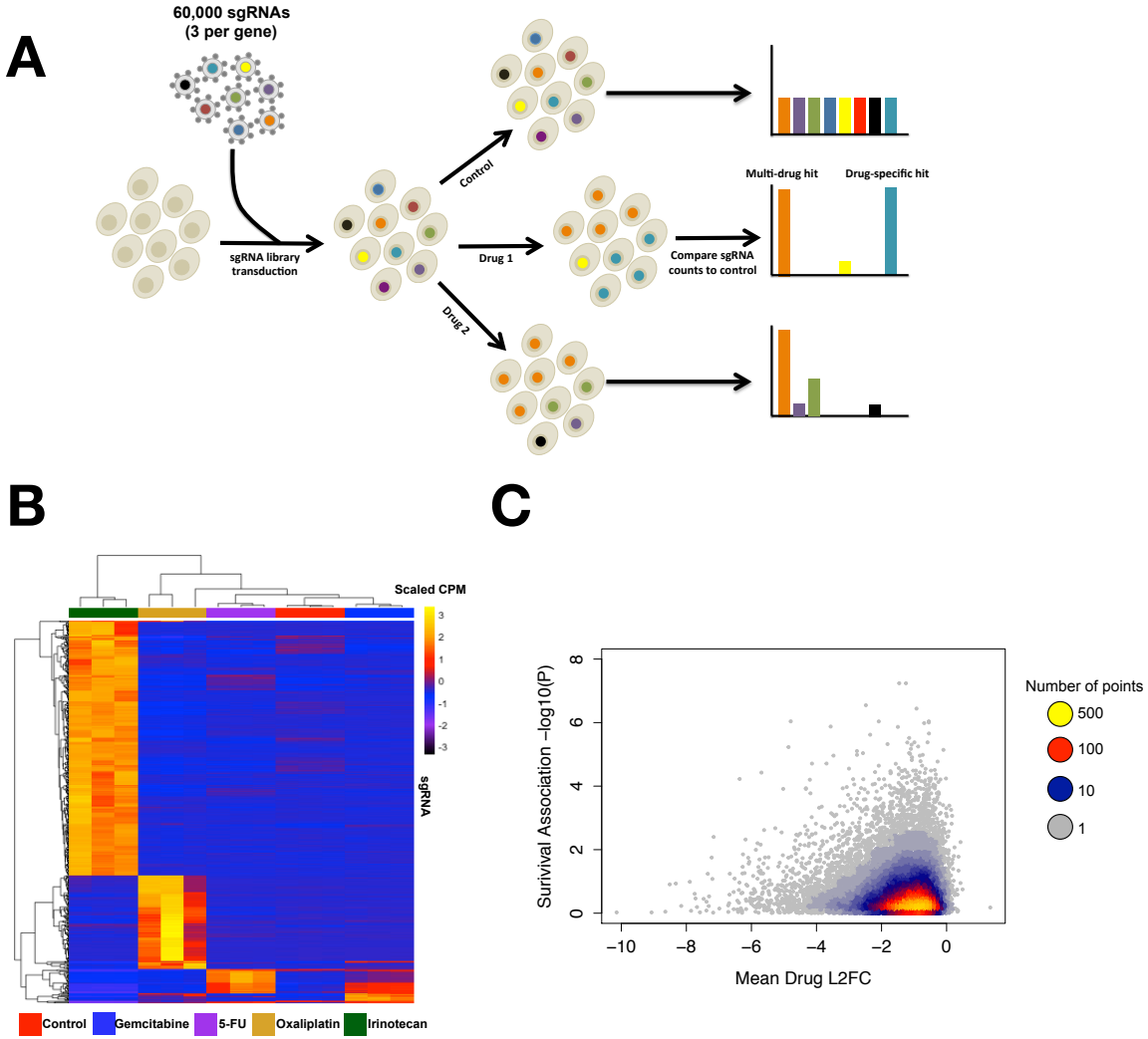
A
60,000 sgRNAs
(3 per gene)
sgRNA library
transduction
Control
Drug 1
Drug 2
Compare sgRNA
counts to control
Multi-drug hit
Drug-specific hit
B
Scaled CPM
3
2
1
0
-1
-2
-3
sgRNA
Control
Gemcitabine
5-FU
Oxaliplatin
Irinotecan
C
Survival Association −log10(P)
0
2
4
6
8
−10
−8
−6
−4
−2
0
Mean Drug L2FC
Number of points
500
100
10
1

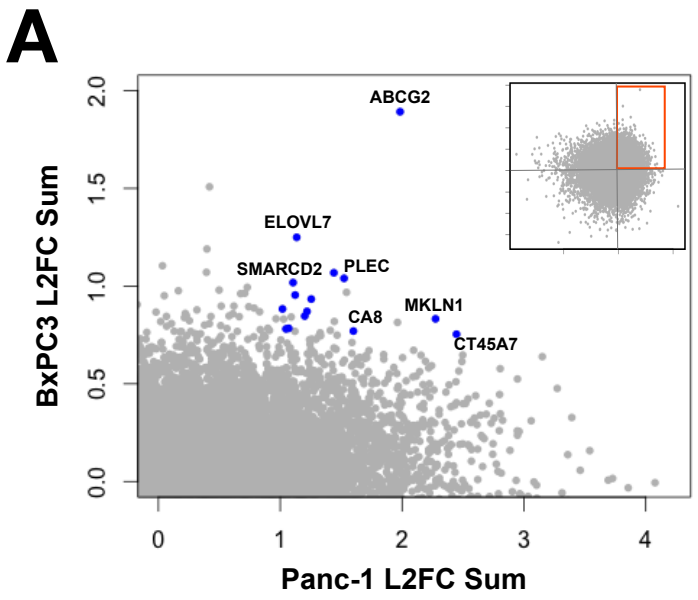
A
ABCG2
ELOVL7
SMARCD2
PLEC
CA8
MKLN1
CT45A7
BxPC3 L2FC Sum
Panc-1 L2FC Sum
0.0
0.5
1.0
1.5
2.0
0
1
2
3
4

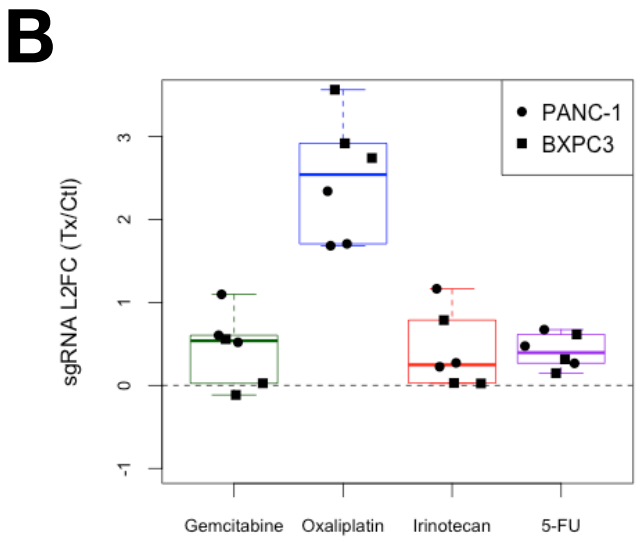
B
PANC-1
BXPC3
sgRNA L2FC (Tx/Ctl)
-1
0
1
2
3
Gemcitabine
Oxaliplatin
Irinotecan
5-FU

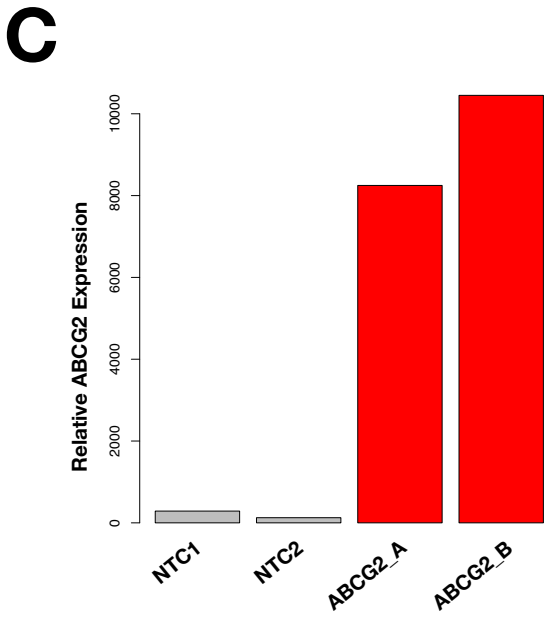
C
Relative ABCG2 Expression
0
2000
4000
6000
8000
10000
NTC1
NTC2
ABCG2_A
ABCG2_B

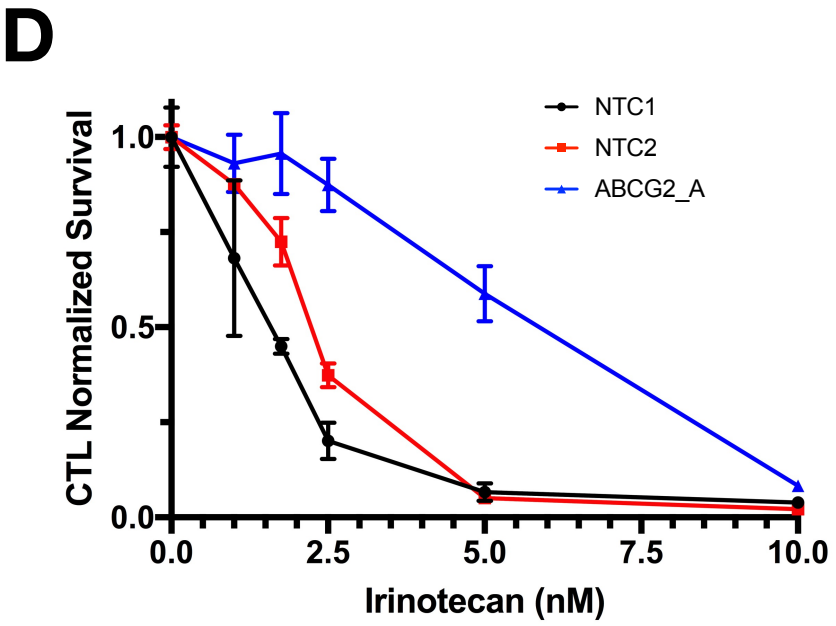
D
NTC1
NTC2
ABCG2_A
CTL Normalized Survival
0.0
0.5
1.0
0.0
2.5
5.0
7.5
10.0
Irinotecan (nM)

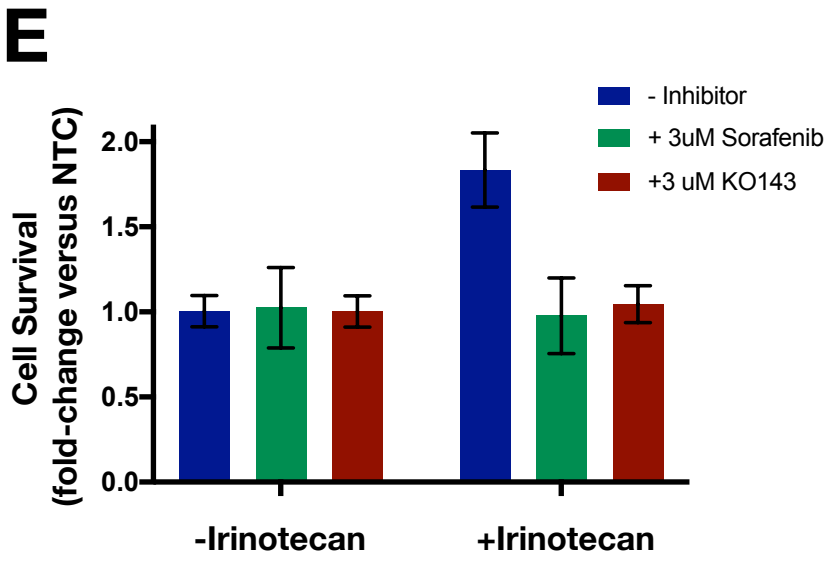
E
- Inhibitor
+ 3uM Sorafenib
+3 uM KO143
Cell Survival
(fold-change versus NTC)
0.0
0.5
1.0
1.5
2.0
-Irinotecan
+Irinotecan

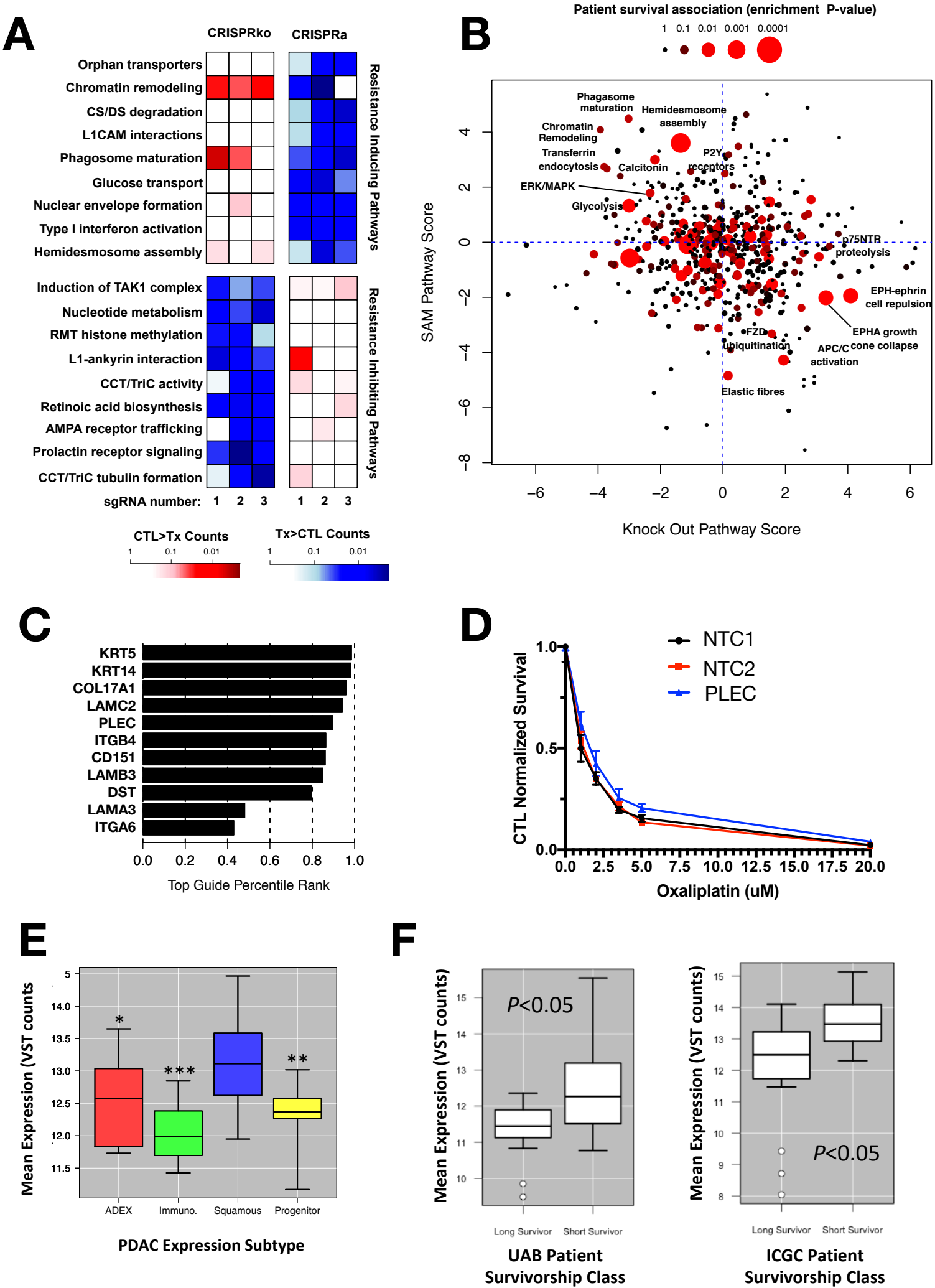
A
CRISPRko
CRISPRa
Orphan transporters
Chromatin remodeling
CS/DS degradation
L1CAM interactions
Phagosome maturation
Glucose transport
Nuclear envelope formation
Type I interferon activation
Hemidesmosome assembly
Resistance Inducing Pathways
Induction of TAK1 complex
Nucleotide metabolism
RMT histone methylation
L1-ankyrin interaction
CCT/TriC activity
Retinoic acid biosynthesis
AMPA receptor trafficking
Prolactin receptor signaling
CCT/TriC tubulin formation
Resistance Inhibiting Pathways
sgRNA number: 1 2 3 1 2 3
CTL>Tx Counts
1 0.1 0.01
Tx>CTL Counts
1 0.1 0.01
B
Patient survival association (enrichment P-value)
1 0.1 0.01 0.001 0.0001
Phagasome maturation
Hemidesmosome assembly
Chromatin Remodeling
Transferrin endocytosis
Calcitonin
P2Y receptors
ERK/MAPK
Glycolysis
p75NTR proteolysis
EPH-ephrin cell repulsion
EPHA growth cone collapse
APC/C activation
FZD ubiquitination
Elastic fibres
SAM Pathway Score
Knock Out Pathway Score
C
KRT5
KRT14
COL17A1
LAMC2
PLEC
ITGB4
CD151
LAMB3
DST
LAMA3
ITGA6
Top Guide Percentile Rank
D
NTC1
NTC2
PLEC
CTL Normalized Survival
Oxaliplatin (uM)
E
Mean Expression (VST counts)
ADEX
Immuno.
Squamous
Progenitor
PDAC Expression Subtype
F
Mean Expression (VST counts)
P<0.05
Long Survivor
Short Survivor
UAB Patient Survivorship Class
ICGC Patient Survivorship Class

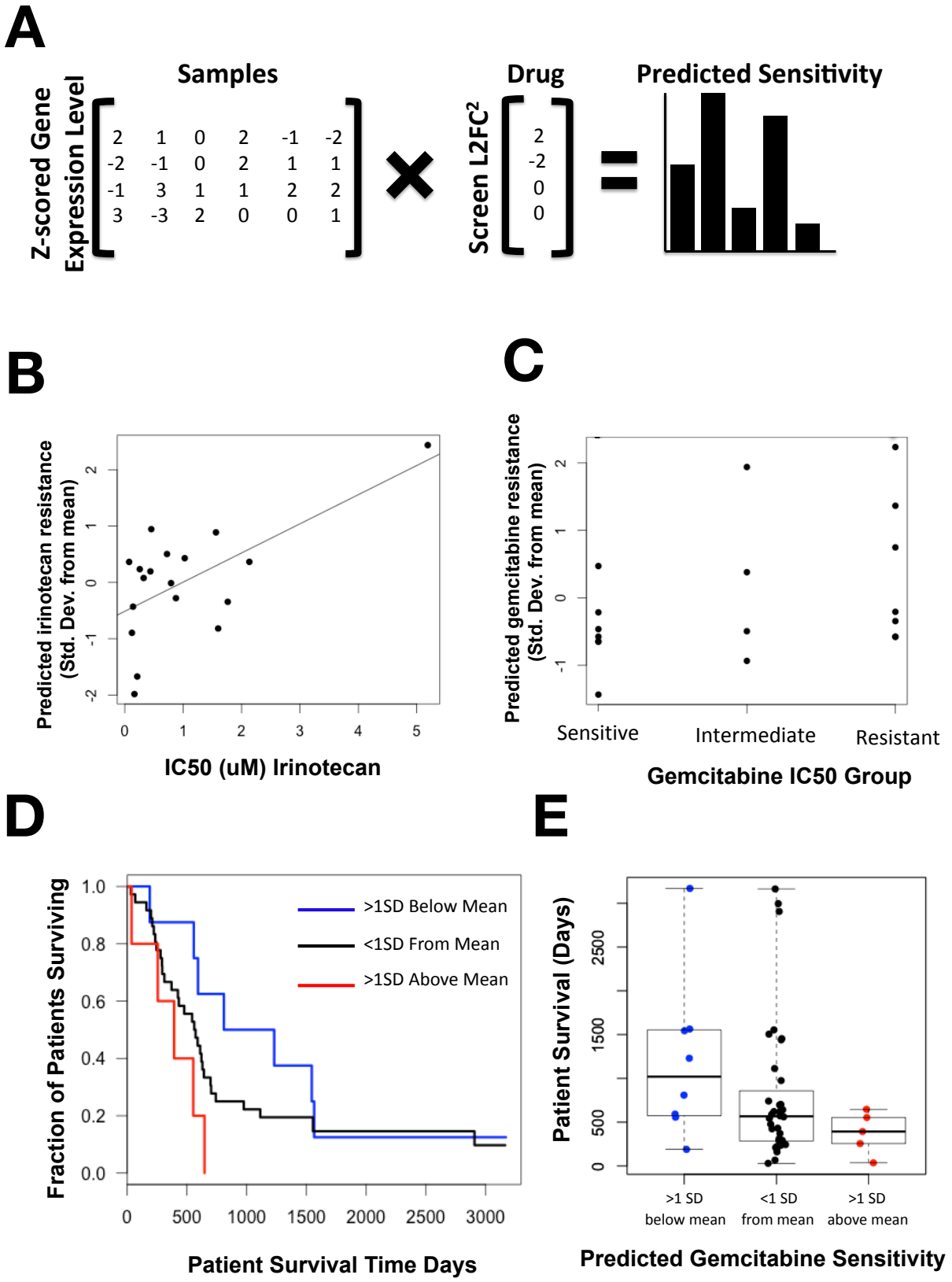
A
Samples
Drug
Predicted Sensitivity
Z-scored Gene Expression Level
2 1 0 2 -1 -2
-2 -1 0 2 1 1
-1 3 1 1 2 2
3 -3 2 0 0 1
Screen L2FC²
2
-2
0
0
B
Predicted irinotecan resistance (Std. Dev. from mean)
IC50 (uM) Irinotecan
C
Predicted gemcitabine resistance (Std. Dev. from mean)
Sensitive
Intermediate
Resistant
Gemcitabine IC50 Group
D
Fraction of Patients Surviving
>1SD Below Mean
<1SD From Mean
>1SD Above Mean
Patient Survival Time Days
E
Patient Survival (Days)
>1 SD below mean
<1 SD from mean
>1 SD above mean
Predicted Gemcitabine Sensitivity